**Nationaal Lucht- en Ruimtevaartlaboratorium**
National Aerospace Laboratory NLR

NLR-TP-2014-146

# A fast atmospheric sound propagation model for aircraft noise prediction

M. Tuinstra

**Nationaal Lucht- en Ruimtevaartlaboratorium**
National Aerospace Laboratory NLR

Anthony Fokkerweg 2
P.O. Box 90502
1006 BM  Amsterdam
The Netherlands
Telephone +31 (0)88 511 31 13
Fax +31 (0)88 511 32 10
www.nlr.nl

**Nationaal Lucht- en Ruimtevaartlaboratorium**

National Aerospace Laboratory NLR

## Executive summary

# A fast atmospheric sound propagation model for aircraft noise prediction

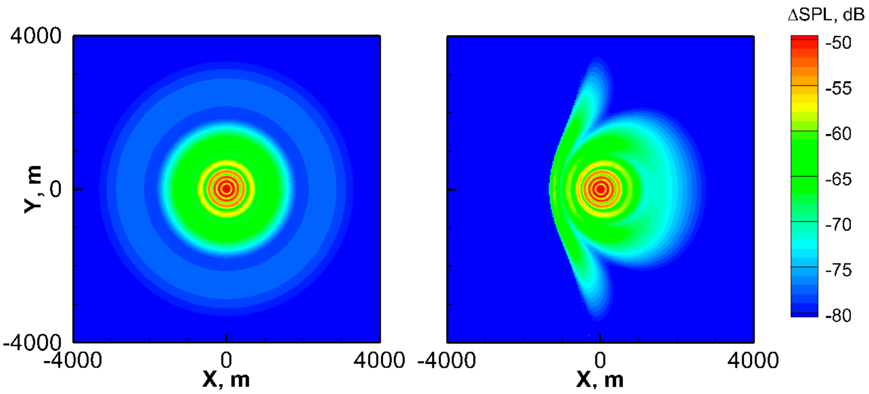


*Uniform atmosphere* *Logarithmic wind profile*

**Report no.**
NLR-TP-2014-146

**Author(s)**
M. Tuinstra

**Report classification**
UNCLASSIFIED

**Date**
October 2015

**Knowledge area(s)**
Aëro-akoestisch en experimenteel aërodynamisch onderzoek

**Descriptor(s)**
Aircraft noise modelling
noise propagation
ray acoustics
refraction


**Problem area**
The effect of the atmosphere on sound propagation can impact the perceived noise on the ground significantly and therefore needs to be accounted for in aircraft noise modelling.

**Description of work**
In order to be practical, propagation modelling cannot impose a limitation on calculation time. The aim is therefore to design a robust and computationally lean atmospheric propagation model for the prediction of aircraft noise. To achieve a computationally low demanding algorithm an analytical approach is pursued.

**Results and conclusions**
When the wave front orientation is approximated to be orientated perpendicular to the ray path, it follows from the Eikonal equation that a ray obeys to an adapted form of Snell's law. If the atmosphere is then discretized in layers of linearly varying sound speed and wind velocity, it allows the ray path and ray properties to be expressed analytically within a layer. Cross-validation against two independently developed ray tracing routines has shown the validity of the selected modelling approach.
In conclusion, a robust and computationally low demanding method has been developed for atmospheric sound propagation that can be incorporated in aircraft noise modelling.

**Applicability**
Foreseen applications are the evaluation of en-route noise, noise optimisation studies and the evaluation of noise in airport scenarios. The tool will be applied for the evaluation of en-route noise that is related to novel engine


This report is based on an article published in the International Journal of Aeroacoustics vol 13 nr 5 & 6 2014, by Multi Science Publishing.

configurations. In the future this tool can furthermore contribute to high-fidelity noise abatement studies and the evaluation of noise contours in airport scenarios, taking into account the effect of realistic meteorological conditions on noise propagation.

**Nationaal Lucht- en Ruimtevaartlaboratorium**, National Aerospace Laboratory NLR

Anthony Fokkerweg 2, 1059 CM Amsterdam,
P.O. Box 90502, 1006 BM Amsterdam, The Netherlands
Telephone +31 88 511 31 13, Fax +31 88 511 32 10, www.nlr.nl

**Nationaal Lucht- en Ruimtevaartlaboratorium**
National Aerospace Laboratory NLR

NLR-TP-2014-146

# A fast atmospheric sound propagation model for aircraft noise prediction

M. Tuinstra

This report is based on an article published in the International Journal of Aeroacoustics vol 13 nr 5 & 6 2014, by Multi Science Publishing.


This publication has been refereed by the Advisory Committee AEROSPACE VEHICLES.

| | |
|---|---|
| Customer | National Aerospace Laboratory NLR |
| Contract number | ----- |
| Owner | NLR |
| Division NLR | Aerospace Vehicles |
| Distribution | Unlimited |
| Classification of title | Unclassified |
| | October 2015 |

Approved by:

| Author | Reviewer | Managing department |
|---|---|---|
| Marthijn Tuinstra | Harry Brouwer | Joost Hakkaart |
| Date: 26-11-2015 | Date: 1-12-2015 | Date: 2/12/15 |

# Contents

This page is intentionally left blank.

# A fast atmospheric sound propagation model for aircraft noise prediction

**Marthijn Tuinstra**
*National Aerospace Laboratories, NLR*
*Voorsterweg 31, 8316 PR Marknesse, The Netherlands*

*Submitted: Oct 8, 2013; Revised May 16, 2014; Accepted Aug 19, 2014*

## ABSTRACT
The effect of the atmosphere on sound propagation can impact the perceived noise on the ground significantly and therefore needs to be accounted for in aircraft noise modelling. However, to be practical, propagation modelling cannot impose a limitation on calculation time. The aim is therefore to design a robust and computationally lean atmospheric propagation model for the prediction of aircraft noise. Foreseen applications are the evaluation of en-route noise, noise optimisation studies and the evaluation of noise in airport scenarios.

To achieve a computationally low demanding algorithm an analytical approach is pursued. When the wave front orientation is approximated to be perpendicular to the ray path, it follows from the Eikonal equation that a ray obeys to an adapted form of Snell's law. If the atmosphere is then discretized in layers of linearly varying sound speed and wind velocity, it allows the ray path and ray properties to be expressed analytically within a layer. Cross-validation against two independently developed ray tracing routines has shown the validity of the selected modelling approach.

In conclusion, a robust and computationally low demanding method has been developed for atmospheric sound propagation that can be incorporated in aircraft noise modelling.

Key words: Aircraft noise modelling, noise propagation, ray acoustics, refraction

## NOMENCLATURE
***Roman symbols***

| | |
|---|---|
| A | ray tube cross sectional surface area |
| $a,b,x$ | constants of a quadratic equation $ax^2 + bx + c$ |
| $c_s$ | speed of sound |
| $c_{eff}$ | effective speed of sound $c_s + v_w$ |
| $c_{perc}$ | perceived speed of sound $c_s + \sin\theta v_w$ |
| $f$ | frequency |

*Corresponding author: E-mail: Marthijn.Tuinstra@nlr.nl

| | |
|---|---|
| $g_0$ | standard gravity |
| $h_{mic}$ | microphone altitude |
| $I$ | measure of constructive/destructive interference |
| $L$ | lapse rate of atmospheric temperature |
| $\mathbf{n}$/n | wavefront normal |
| $O$ | observer position |
| $p$ | acoustic pressure amplitude |
| $P$ | atmospheric pressure |
| $q_c$ | linear coefficient of speed of sound |
| $q_v$ | linear coefficient of wind velocity |
| $q_\zeta$ | linear coefficient of an arbitrary linear variable $\zeta$ |
| $R$ | square root of a quadratic equation $\sqrt{ax^2+bx+c}$ |
| $R_p$ | planar reflection coefficient |
| $R_{sp}$ | specific gas constant in air |
| $S$ | source position |
| $s$ | curvilinear coordinate along a ray path |
| $t$ | wavefront travel time |
| $T$ | atmospheric temperature |
| $\mathbf{v}$/v | velocity vector/component |
| $v_w$ | wind velocity |
| $\mathbf{x}$ | cartesian coordinate vector |
| $x,y$ | ray coordinates |
| $X,Y,Z$ | global coordinates |
| $Z_s$ | surface impedance |

*Greek symbols*

| | |
|---|---|
| $\Delta$ | difference |
| $\theta$ | ray path angle |
| $\gamma$ | heat capacity ratio |
| $\rho$ | air density |
| $\sigma$ | flow resistivity |
| $\tau$ | eikonal |
| $\zeta$ | arbitrary linear variable |
| $\omega$ | angular frequency |
| $\xi$ | phase of complex reflection coefficient $R_p$ |

*Subscripts*

| | |
|---|---|
| $_0$ | initial condition, e.g. $\theta_0$ initial ray path angle |
| $_1$ | observer condition |
| $_\mathrm{c}$ | centre frequency |
| $_\mathrm{d}$ | direct wave |
| $_i$ | layer index |
| $_f$ | curve fit |
| $_m$ | valve |

| | |
|---|---|
| *obs* | observer |
| r | reflected wave |
| *ref* | reference |
| *rt* | root |
| *src* | source |
| *srfc* | surface |
| *true* | true distance |
| *x, y, z* | x, y or z component |

*Abbreviations*

| | |
|---|---|
| ISA | international standard atmosphere |
| PBL | planetary boundary layer |
| SPL | sound pressure level |

## 1. INTRODUCTION

Aircraft noise propagation is affected by ground- and meteorological effects for which must be accounted for in aircraft noise predictions. The need to incorporate this in prediction models was already recognized in the 1980s by the SAE engineering society[1], whom developed an empirical lateral attenuation model that implicitly includes these effects. Up to this day this relatively crude but fast lateral attenuation model is still regularly applied in aircraft noise prediction suites.

Last decade, several European research initiatives have been deployed to improve aircraft noise modelling. SOPRANO (Silencer cOmmon PlatfoRm for Aircraft NOise calculations) was developed in the SILENCER project and aimed at providing a common European platform for fixed wing aircraft noise predictions. HELENA (HELicopter Environmental Noise Analysis) was developed in the FRIENDCOPTER project with the goal of improving helicopter noise predictions. For both tools the necessity was identified for an accurate propagation model that takes into account atmospheric refraction due to speed of sound and wind velocity gradients.

The development of APHRODITE (AtmosPHeric RefractiOn preDIcTion mEthod) was initiated in the SILENCER project and completed in the European project NINHA (Noise Impact of aircraft with Novel engine configurations in mid- to High Altitude operations) for the purpose of prediction of en-route noise. Other envisioned applications are noise optimisation studies and the evaluation of noise in airport scenarios. An example of the former is the use of genetic algorithms that require a large number of calculations to obtain a noise optimized flight path in an iterative manner. In the latter case aircraft movements at an airport for an entire year (~400000 for a large hub) need to be evaluated. The objective of APRHODITE is therefore to provide a robust and computationally low demanding atmospheric propagation model for the prediction of aircraft noise.

The article is outlined as follows. Section 2 and 3 treat the fundamentals of sound propagation in the atmosphere. These fundamentals provide the backbone of the atmospheric propagation model that is presented in section 4. The noise propagation model is evaluated in section 5. A cross-validation is carried out with independently developed propagation models and furthermore, the computational cost of the model is assessed. Section 6 summarises the conclusions.

# 2. SOUND PROPAGATION IN THE ATMOSPHERE

## 2.1. The atmosphere

The earth's atmosphere consists of a layer of gasses surrounding the planet, captured by its gravitational pull. The physical and chemical properties of air change as the altitude above the earth's surface is increased. The International Standard Atmosphere[2] (ISA) attempts to capture this in a model that divides the atmosphere in layers of linear varying temperature (Figure 1). Cruise altitude of most commercial airliners is at about 11km (Tropopause). At this altitude meteorological disturbances are small, the drag is low and the gas turbine engines function optimally. Therefore, for aircraft noise modelling the Troposphere is of most relevance.

The Troposphere is the layer closest to the earth's surface in which the temperature decreases with altitude (–0.0065°K/m). The Troposphere is divided in two regions: the Free Atmosphere and the Planetary Boundary Layer (PBL). The Planetary Boundary Layer covers the lowest 1km-2km where the atmosphere is directly affected

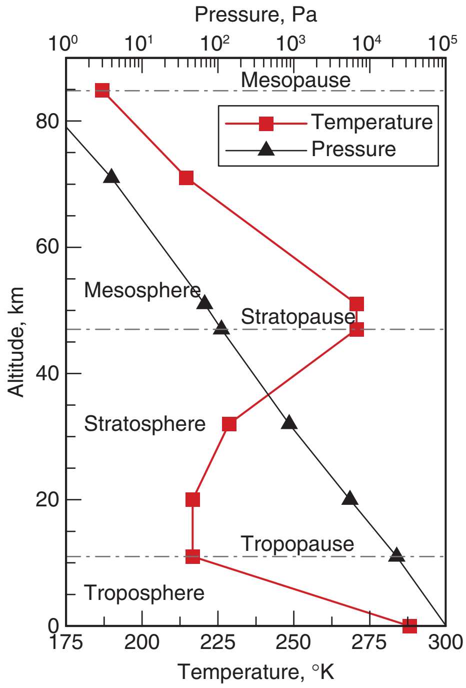


**Figure 1:** ISA atmosphere, temperature and pressure with altitude.

by the presence of the earth's surface. The PBL is typically turbulent and characterized by a vertical exchange of momentum, heat and moisture. In the surface layer (or constant flux layer) covering the lowest 10% of the PBL, the strongest gradients in both temperature and velocity are found and the effect of the earth's rotation on wind is negligible. An example of typical wind velocity, temperature and speed of sound profiles occurring near the surface is shown in Figure 2. The velocity gradient results from friction forces arising due to the presence of the earth's surface, eventually reducing the wind velocity to zero at the surface itself (no-slip-condition, $V_w$=0m/s). The velocity typically follows a logarithmic profile and is approximately unidirectional (see Monin and Obukhov [3]). The surface stress, vertical heat flux and terrain roughness are the parameters that govern the shape of average velocity profile. Strong temperature gradients can arise due to changes of the surface temperature. For example, for a warm summer day after sun-set the surface cools down more rapidly than the atmosphere. This results in a temperature inversion that stabilizes the surface layer and is most profound at sun-rise (after which the surface is reheated). The effect of the atmosphere on sound propagation is therefore in particular of relevance for landing and take-off operations of aircraft, since sound propagation will take place almost entirely within the surface layer.

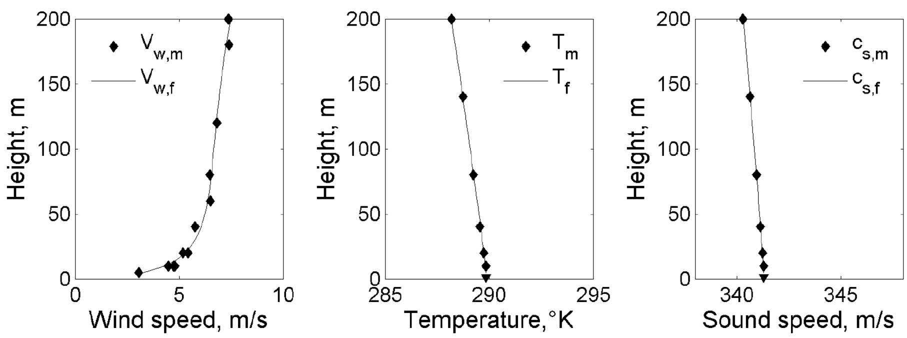


**Figure 2:** Typical wind velocity profile (left), temperature profile (centre) and related sound speed profile (right) measured at the Cabauw tower of the Royal Netherlands Meteorological Institute (KNMI), symbols represent measured values, solid lines are fitted to the data

The upper part of the PBL (Mixed Layer) connects the Surface Layer to the Free Atmosphere and both friction and Coriolis forces (an apparent force that arises due to rotation of the earth) play a role. The wind direction is no longer uniform as it turns to adapt to the geostrophic currents encountered in the Free Atmosphere. In the Free Atmosphere the effect of earth's surface on wind is negligible and the pressure gradient forces are entirely balanced by the Coriolis forces. When this occurs the wind is considered geostrophic, which means that the direction of the flow is parallel with isobars. In northern hemisphere this results in a counter clockwise wind around an area of low pressure. Both situations as encountered in the Free Atmosphere and Mixed Layer are depicted in Figure 3. A more detailed discussion on boundary layer meteorology can be found for example in the work of Bull [4].

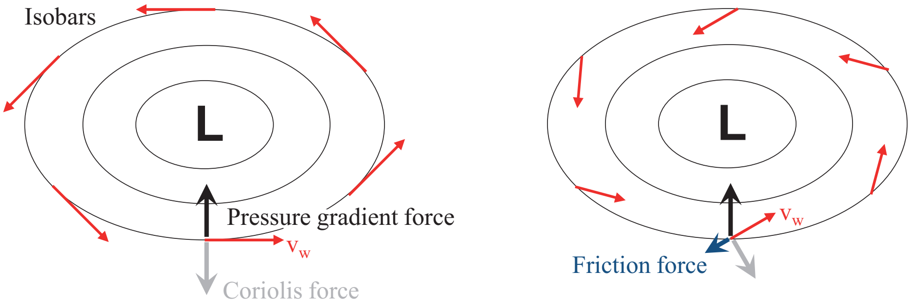


**Figure 3:** Low-pressure area in the northern hemisphere, left: in the Free Atmosphere the pressure gradient forces are entirely balanced by Coriolis forces causing wind the flow along isobars (geostrophic currents). Right, in the Mixed Layer friction reduces the wind velocity and hence Coriolis force, destroying the geostrophic balance and allowing wind to cross isobars

## 2.2. Sound propagation

Temperature, wind velocity and wind direction vary throughout the atmosphere and hence can be expected to affect sound propagation. The scales at which these variations occur are hundreds of meters, far greater than a typical acoustic wavelength. This makes the sound propagation through an atmosphere ideally suited to be treated with ray theory. The concept of rays has been adapted to acoustics from light wave propagation theory and allows wave propagation to be described in terms of ray paths, provided that the variations of the medium occur over a length scale far greater than the wavelength. As pointed out by Dowling et al. [5], in this case the only effect of variations in sound speed is that the speed of propagation of a wavefront varies along the ray and the amplitude of the wave changes slowly. The process is entirely governed by refraction and locally, at the scale of an acoustic wavelength, the wavefront appears planar.

The eikonal equation lies at the core of ray tracing as it describes the wavefronts and ray paths:

$$(\nabla\tau)^2 = \frac{1}{(c_s + \mathbf{v}\cdot\mathbf{n})^2} \tag{1}$$

In this $\tau(\mathbf{x})$ is the eikonal (or phase function) that describes surfaces of constant phase, i.e. wave fronts (see Figure 4). On the right hand side $c_s$ is the sound speed, $\mathbf{v}$ the

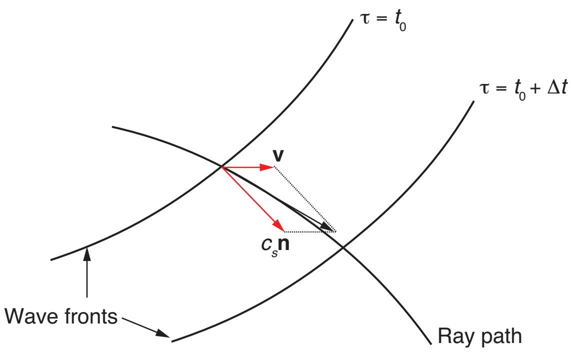


**Figure 4:** Ray path in an inhomogeneous medium.

wind velocity and **n** the wavefront normal. For a full derivation of the eikonal equation, refer to Pierce et al. [6].

Dowling et al. [5] derive in chapter 5.2 that a ray propagating in a stratified medium with varying sound speed obeys Snell's law, which dictates that $\sin\theta/ c_s$ = constants along a ray. We will follow similar arguments to derive a relation that holds in a moving medium. First the assumption is made that a ray follows a path that is perpendicular to the wave fronts. Although Figure 4 shows that this is not strictly the case for a convecting medium, it is deemed an acceptable approximation for atmospheric propagation since the wind velocity is generally much smaller than the speed of sound ($v_w/c_s$ <<1). The relevant ray coordinates are then given in Figure 5.

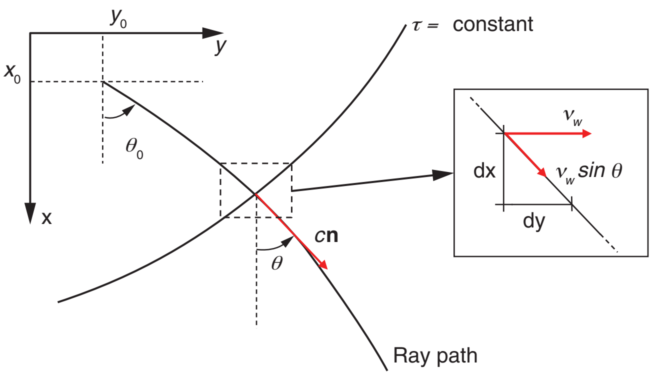


**Figure 5:** Ray coordinates, x,y are carthesian coordinate and θ the ray path angle with respect to the x-axis.

For the subsequent analysis the ray path is assumed to be confined to the x-y plane. The wave front normal

$$\mathbf{n} = \frac{\nabla\tau}{|\nabla\tau|} \tag{2}$$

is obtained from the eikonal. Since a stratified atmosphere is assumed $v_y = v_w$(x) only, where $v_w$ is the wind velocity, and $v_x = 0$ m/s. From eq. (2) it follows that:

$$\frac{n_y}{c_s + \mathbf{v}\cdot\mathbf{n}} = \frac{\sin\theta}{c_s + \sin\theta\, v_w} = \frac{\partial\tau}{\partial y} \tag{3}$$

If $s$ is defined as a curvilinear coordinate along the ray path, then taking the derivative with respect to $s$ yields:

$$\frac{d}{ds}\left(\frac{\sin\theta}{c_s + \sin\theta\, v_w}\right) = \frac{d}{ds}\frac{\partial\tau}{\partial y} = 0 \tag{4}$$

That the right hand side equals zero is proven as follows:

$$\begin{aligned}\frac{d}{ds}\frac{\partial\tau}{\partial y} &= \left(n_x\frac{\partial}{\partial x} + n_y\frac{\partial}{\partial y}\right)\frac{\partial\tau}{\partial y}\\ &= \left(c_s + v_w\sin\theta\right)\left(\frac{\partial\tau}{\partial x}\frac{\partial}{\partial x} + \frac{\partial\tau}{\partial y}\frac{\partial}{\partial y}\right)\frac{\partial\tau}{\partial y}\\ &= \left(c_s + v_w\sin\theta\right)\left(\frac{\partial\tau}{\partial x}\frac{\partial^2\tau}{\partial y\partial x} + \frac{\partial\tau}{\partial y}\frac{\partial^2\tau}{\partial y^2}\right)\\ &= \left(c_s + v_w\sin\theta\right)\frac{\partial}{\partial y}\left(\left(\frac{\partial\tau}{\partial x}\right)^2 + \left(\frac{\partial\tau}{\partial y}\right)^2\right)\end{aligned} \tag{5}$$

In which $n_x$ and $n_y$ are the normal components in x and y direction given by eq.(2). Substitution of eq. (1) in eq. (5) and the fact that the velocity and speed of sound is only a function $x$, results in the right hand side of eq. (4) to be zero. Therefore

$$\frac{\sin\theta}{c_s + \sin\theta\, v_w} = \text{constant} \tag{6}$$

along a ray. Intuitively this can be understood as only the wavefront normal component of wind velocity affecting sound refraction. This relation forms the basis for the atmospheric propagation model presented in next sections. For near horizontal wave propagation, a further approximation is often made that sin $\theta \approx 1$ in the denominator. In this case the ray undergoes refraction due to wind gradient as it would by a speed of sound gradient with an effective sound speed of $c_{eff} = c_s + v_w$. Since aircraft noise deals with air-to-ground propagation, the effective sound speed approximation is not applicable. To avoid possible confusion in the remainder of the article $c_s + \sin\theta\, v_w$ will be referred to as the perceived sound speed ($c_{perc}$).

## 3. RAY TRACING IN A MEDIUM WITH LINEARLY VARYING VELOCITY AND SPEED OF SOUND

### 3.1. Ray path

Let $y = y(x)$ be the equation that specifies the ray path emanating from $(x,y) = (x_0,y_0)$ with an angle $\theta_0$ with respect to the vertical axis (see Figure 5). It then follows from eq. (6) that along this ray:

$$\sin\theta = \frac{c_s \sin\theta_0}{c_0 + \sin\theta_0\left(v_0 - v_w\right)} \tag{7}$$

where $c_0$ and $v_0$ are the speed of sound at $x_0$ and wind velocity at $x_0$ respectively. The left hand side of eq. (7) is expressed in infinitesimals

$$\sin\theta = \frac{dy}{\left(\left(dy\right)^2 + \left(dx\right)^2\right)^{1/2}} \tag{8}$$

and a linear varying speed of sound and wind velocity is assumed:

$$\begin{aligned} c_s &= c_0 + q_c x \\ v_w &= v_0 + q_v x \end{aligned} \tag{9}$$

in which $q_c$ and $q_v$ are linear coefficients of speed of sound and wind velocity. This allows eq. (7) to be expressed in form of an ordinary differential equation

$$\frac{dy}{dx} = \pm \frac{\sin\theta_0\left(c_0 + q_c x\right)}{\left(\left[c_0 - \sin\theta_0 q_v x\right]^2 - \sin^2\theta_0\left[c_0 + q_c x\right]\right)^{1/2}} = \pm\sin\theta_0\left\{\frac{c_0}{R} + \frac{q_c x}{R}\right\} \tag{10}$$

in which

$$\begin{aligned} &R = \sqrt{ax^2 + bx + c} \\ &\text{with} \\ &a = \sin^2\theta_0\left(q_v^2 - q_c^2\right) \\ &b = -2c_0\sin\theta_0\left(q_v + \sin\theta_0 q_c\right) \\ &c = c_0^2\left(1 - \sin^2\theta_0\right) \end{aligned} \tag{11}$$

A set of standard integrals (see Appendix) is used to solve above differential equation, to yield an analytical solution

$$y(x) = \pm\sin\theta_0\left(c_0 - \frac{b}{2a}q_c\right)\int_{x_0}^{x}\frac{dx}{R} \pm \sin\theta_0 q_c\frac{R-R_0}{a} \tag{12}$$

that represents the ray path equation. Figure 6 shows typical ray paths with as aim to single out some striking features.

On the left a ray path is plotted for an atmosphere of linearly varying speed of sound that increases in positive x-direction ($q_v = 0.02$,b $c_0 = 242.5$m/s) and no wind. The ray is launched in the positive x direction with an initial angle of $\theta_0 = 45°$ (indicated by the diamond symbol). The ray path is deflected away from the x-axis as it moves in positive x direction and forms a circular path in correspondence of what is described in works of reference[5,6]. The + branch corresponds to ray path angles $-90°<\theta \leq 90°$, whereas the - branch represents $90°<\theta \leq 180° \cup -90° \geq \theta > -180°$. An interesting particularity is that it would take infinite amount of time for a wavefront to achieve a vertical orientation, where $c_s = 0$m/s. The upper part of the circle does not represent a physical solution as in this region the speed of sound attains negative values.

On the right of Figure 6 a ray path is plotted for an atmosphere of constant speed of sound and increasing wind velocity in positive x-direction ($q_v = 0.02$). The ray is launched with an initial angle of $\theta_0 = 45°$ (again indicated by a diamond symbol). Increasing velocity similar to an increasing sound speed, leads to a deflection away from the x-axis. The ray path is no longer circular and in the limit for x → –∞ the ray approaches a vertical orientation (perpendicular to the gradient direction) under which condition the ray no longer undergoes refraction. The lower part of the figure shows an

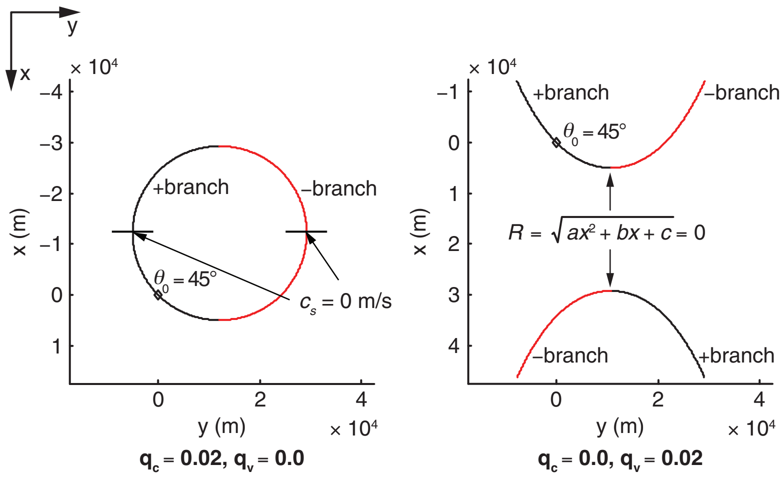


**Figure 6:** Ray path in an atmosphere with linearly varying sound speed (left) and linearly varying wind speed (right).

unconnected solution branch. This corresponds to a solution for negative ray angles, or in other words upstream propagation. A ray however, will never change direction from up-wind to down-wind propagation, or vice versa, hence the unconnected solution branches.

Finally, it is noted that the ray inflection points can be found a-priory. From eq. (10) it follows that they correspond to the x-coordinate where $R = 0$:

$$x_{rt1,rt2} = \frac{-b \pm \sqrt{b^2 - 4ac}}{2a} \tag{13}$$

Furthermore, the ray paths are mirror symmetric about $y = y_{rt}$.

### 3.2. Wave front travel time

If one were to follow a wavefront ($\tau$ = constant) along a ray, then the wavefront travel time is defined as the time it takes to travel a distance $s$, where $s$ is a curvilinear coordinate parallel to the ray path. The perceived speed of sound speed ($c_{perc}$) from a fixed point of reference, i.e. an observer not moving with the medium itself, is $c_s + \sin\theta\, v_w$. Therefore the time needed to travel an infinitesimal distance $ds$ along the ray is given by

$$dt = \frac{ds}{c_{perc}} \tag{14}$$

Using eq. (10) $ds$ can be expressed as

$$ds = \sqrt{dx^2 + dy^2} = \sqrt{1 + \left(\frac{dy}{dx}\right)^2}\, dx = \frac{c_0 - \sin\theta_0 q_v x}{R} \tag{15}$$

Furthermore, by virtue of eq. (7) the perceived sound speed can be written as

$$c_{perc} = c_s + \sin\theta v_w = \frac{c_s}{c_0 - \sin\theta_0 q_v x}\left(c_0 + \sin\theta_0 v_0\right) \tag{16}$$

Substitution of eq. (15) and eq. (16) into eq. (14) then yields

$$dt = \frac{\left(c_0 - \sin\theta_0 q_v x\right)^2}{Rc_s\left(c_0 + \sin\theta_0 v_0\right)} dx \tag{17}$$

This equation can be solved using standard integrals that are provided in the Appendix. After some straightforward but tedious manipulations this will give:

$$
\begin{aligned}
t = &\frac{c_0^2\left(\sin\theta_0 q_v + q_c\right)^2}{\left(c_0+\sin\theta_0 v_0\right)q_c^2}\int_{c_0}^{c_s}\frac{dc_s}{c_s R} \\
&-\frac{c_0\sin\theta_0 q_v\left(\sin\theta_0 q_v + q_c\right)\left(q_v^2-2q_c^2\right)}{q_c^2\left(c_0+\sin\theta_0 v_0\right)\left(q_v^2-q_c^2\right)}\int_{x_0}^{x}\frac{dx}{R}+\frac{q_v^2}{\left(c_0+\sin\theta_0 v_0\right)q_c\left(q_v^2-q_c^2\right)}\left(R-R_0\right)
\end{aligned}
\tag{18}
$$

in which

$$
\int_{c_0}^{c_s}\frac{dc_s}{c_s R} = -\frac{1}{c_0\left(\sin\theta_0 q_v + q_c\right)}\ln\left(\frac{R+c_0-\sin\theta_0 q_v x}{\left(c_0+q_c x\right)\left(\sqrt{1-\sin^2\theta_0}+1\right)}\right) \tag{19}
$$

## 3.3. Averaged parameters

In the atmosphere environmental variables such as pressure, temperature or relative humidity vary with altitude. A linear relation with x is assumed:

$$
\zeta = \zeta_0 + q_\zeta x \tag{20}
$$

for an generic variable $\zeta$, where $q_\zeta$ is a linear coefficient. Since the ray path is curved and the perceived sound speed varies with $x$ and ray orientation, a straightforward spatial average is not adequate. The average value $\bar{\zeta}$ experienced by a wavefront propagating along the ray is given by:

$$
\bar{\zeta} = \frac{1}{\left(t-t_0\right)}\int_{t_0}^{t}\zeta\, dt = \zeta_0 - \frac{q_\zeta c_0}{q_c} + \frac{q_\zeta}{q_c\left(t-t_0\right)}\int_{t_0}^{t} c_s\, dt \tag{21}
$$

Now, if eq. (17) is substituted in eq. (21) the following equation is obtained:

$$
\bar{\zeta} = \zeta_0 - \frac{q_\zeta c_0}{q_c} + \frac{q_\zeta}{q_c\left(t-t_0\right)\left(c_0+\sin\theta_0 v_0\right)}\int_{x_0}^{x}\frac{\left(c_0-\sin\theta_0 q_v x\right)^2}{R}dx \tag{22}
$$

in which (see Appendix)

$$
\begin{aligned}
\int_{x_0}^{x}\frac{\left(c_0-\sin\theta_0 q_v x\right)^2}{R}dx = &\left\{c_0^2+\frac{\sin\theta_0 q_v c_0 b}{a}+\sin^2\theta_0 q_v^2\frac{3b^2-4ac}{8a^2}\right\}\int_{x_0}^{x}\frac{dx}{R} \\
&-\left\{\frac{3b\sin^2\theta_0 q_v^2}{4a^2}+\frac{2\sin\theta_0 q_v c_0}{a}\right\}\left(R-R_0\right)+\frac{\sin^2\theta_0 q_v^2 x}{a}R
\end{aligned}
\tag{23}
$$

### 3.4. Travelled distance

Equation  can be integrated to obtain the ray path length. For a medium at rest ($v_w$ = 0m/s) this would correspond to the travelled distance of a wavefront. For a convective medium however, the displacement of the medium itself needs to be accounted for. In down-wind direction the travelled distance is shorter than the ray path length and in up-wind direction it is longer.

The travelled distance $s_{true}$ is obtained by time-integration of the speed of sound at which a wavefront travels along the ray path. This is given by

$$s_{true} = \int_{t_0}^{t} c_s \, dt = \left(t - t_0\right)\overline{c}_s \tag{24}$$

, where $\overline{c}_s$ is obtained through eq. (22).

## 4. ATMOSPHERIC PROPAGATION MODEL

### 4.1. Layered atmosphere

The atmosphere is discretized in layers (Figure 7) of linearly varying temperature, velocity and relative humidity, which are provided as input to the model. The wind direction can be uniform or defined separately for each layer. From the temperature $T$ at the layer interfaces, the pressure $p$ and speed of sound $c_s$ is calculated through the relations:

$$c_{s,i} = \sqrt{\gamma R_{sp} T_i} \tag{25}$$

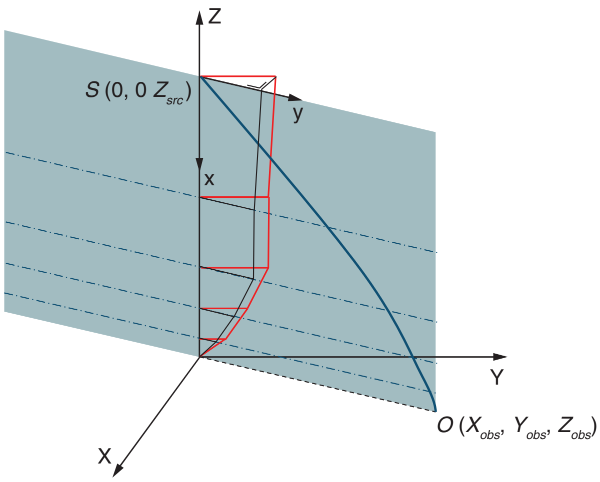


**Figure 7:** A 3D atmosphere projected on a 2D plane.

and

$$\frac{P_{i+1}}{P_i} = \left(\frac{T_{i+1}}{T_i}\right)^{-\frac{g_0}{L_i R_{sp}}} \tag{26}$$

where the subscript $i$ referes to the layer index, $\gamma$ is the heat capacity ratio, $g_0$ the standard gravity, $R_{sp}$ is the specific gas constant in air and $L_i$ the lapse rate in the layer under consideration.

In order to carry out the ray calculations a coordinate transformation is made from global coordinates ($X,Y,Z$) to local ray coordinates ($x,y$). The ray coordinates lay in a plane that is parallel to the Z-axis that contains both the observer ($X_{obs}$, $Y_{obs}$, $Z_{obs}$) and source ((0, 0, $Z_{src}$), Figure 7). The 3D velocity profile is decomposed in a refractive in-plane and non-refractive out-of-plane component. The out-of-plane ray displacement due wind velocity is relatively small since $v_w/c_s$<<1 and is therefore neglected. The ray path and properties can now be described analytically within each layer by the theory presented in the section 3.

## 4.2. Shadow zones and ray matching procedure

Equation (12) describes the ray path for a prescribed initial ray angle $\theta_0$ for given meteorological conditions. In aircraft noise predictions however, often the inverse problem is posed: Which initial ray angle $\theta_0$ is required for a given source and observer? This question can only be answered through an iterative procedure.

Before commencing this procedure, it should be tested if the observer is located in a shadow zone. A shadow zone is an area where rays cannot reach and hence no solution exists. Shadow zones occur for concave ray paths as shown in Figure 8 where the presence of the surface blocks rays from reaching the shadow zone.

Alternatively a pseudo shadow zone occurs if the atmosphere is such that the ray curvature changes from concave to convex (Figure 8, right). It is referred to a pseudo shadow zone since in theory rays can reach this area, however strongly diverge as $\theta_{0,\,max}$ is approached. Similarly to a true shadow zone, noise levels are strongly reduced. Furthermore, computers do not possess infinite precision and therefore it poses a practical constraint on the model algorithm.

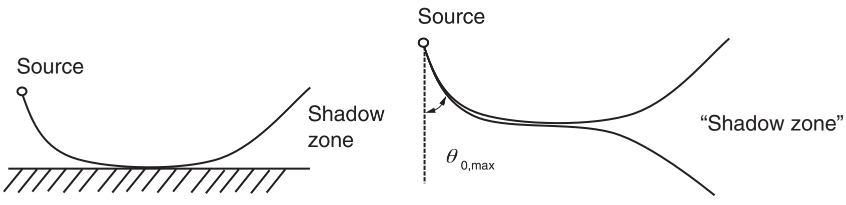


**Figure 8:** Example of a shadow zone (Left) and pseudo shadow zone (right)

The limiting ray can be found through eq. (7). The first consideration to be made is that any inflection point along a ray occurs at $\theta$ = 90° and therefore:

$$\sin\theta_0 = \frac{c_0}{c_{eff} - v_0} \tag{27}$$

Inspection of eq. (27) shows that the inflection point associated with the maximum effective sound speed ($c_{eff} = c_s + v_w$), defines the limiting ray launch angle:

$$\theta_{0,\max} = \arcsin\left(\frac{c_0}{c_{eff,\max} - v_0}\right) \tag{28}$$

If the maximum effective sound speed occurs at the surface the situation as sketched in the left of Figure 8 takes place, otherwise the situation as sketched on the right occurs.

When it is confirmed that required observer position is not in a shadow zone, a root finding algorithm can be used to find the launch angle that matches the observer position $y_{obs}$, by formulating the problem as

$$\left\{y(\theta_0) - y_{obs}\right\}_{x=h_{mic}} = 0 \tag{29}$$

Brent's method[7] is recommended since it combines robust (bisection) and fast (inverse quadratic interpolation, secant method) root finding algorithms and automatically selects the optimal algorithm for the occasion. The method is guaranteed to converge.

### 4.3. Pressure amplitude

The pressure amplitude is calculated by invoking conservation of energy within a ray tube, from which follows that

$$\left(p'^2 A/\rho c_s\right)_{ref} = \left(p'^2 A/\rho c_s\right)_{obs} \tag{30}$$

where $A$ is the ray tube cross sectional surface area. The reference distance $R_{ref}$ is chosen sufficiently close to the source so that any meteorological effects can be neglected. The surface element spanning from $\varphi$, $\varphi + \delta\varphi$ to $\varphi$, $\varphi + \delta\varphi$ is then given by

$$A_{ref} = R_{ref}^2 \sin\theta_0 \delta\theta\delta\varphi \tag{31}$$

To obtain the surface area at the observer location a second ray is launched at an incrementally increased launch angle $\theta + \delta\theta$, which leads to a displacement $\Delta$y as is shown in Figure 9.

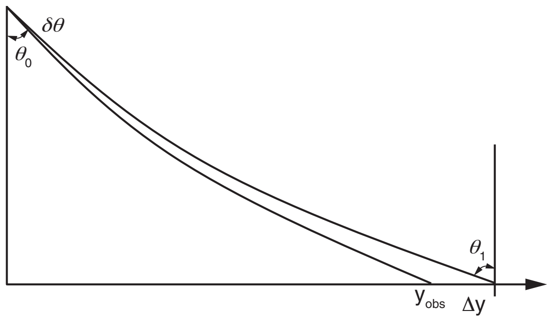


**Figure 9:** Parameters related to pressure amplitude calculation.

The cross-sectional surface area of the ray tube at the observer is obtained from

$$A_{obs} = \Delta y \cos\theta_1 y_{obs} \delta\varphi \tag{32}$$

The decrease in sound pressure level with respect to a reference distance $R_{ref}$ = 1m is then given by

$$\Delta SPL = 10\log\frac{\sin\theta_0\delta\theta}{y_{obs}\Delta y\cos\theta_1} + 10\log\frac{\rho_{obs}c_{s,obs}}{\rho_{ref}c_{s,ref}} \tag{33}$$

## 4.4. Ground reflection and atmospheric attenuation

Ray tracing is a high frequency approximation, but in itself independent of frequency similar to spherical spreading. Atmospheric attenuation and interference or attenuation due to ground reflection is however frequency dependent.

For atmospheric attenuation the model of Bass et al. [8] is used, although several alternative models are available[9,10] that could serve as a substitute. For each layer the attenuation coefficients are calculated based on the average value of pressure, temperature and relative humidity that a wavefront experiences propagating along the ray, which is given by eq. (22). Subsequently, the atmospheric attenuation factor is obtained considering the travelled distance defined by eq. (24).

Ground reflection is modelled as plane wave reflection on an impedance surface assuming zero wind velocity at the surface. A single parameter empirical impedance model by Delany and Bazley [11] is used. Using a $-i\omega t$ convention this is given by:

$$Z_s = 1 + 0.0511\left(\frac{f}{\sigma}\right)^{-0.754} + i0.0768\left(\frac{f}{\sigma}\right)^{-0.732} \tag{34}$$

in which $f$ is the frequencdy and $\sigma$ is the flow resistivity. Typical values of $\sigma$ for commonly occurring natural surfaces are found in Table 1.

More complex impedance models[12] could be used. However those models also require detailed knowledge of surface under consideration, which is generally not available.

The complex plane wave reflection coefficient is obtained through

$$R_p = \frac{Z_s \cos\theta_{srfc} - 1}{Z_s \cos\theta_{srfc} + 1} \tag{35}$$

where $\theta_{srfc}$ is the ray surface impingement angle. Now consider a direct wave and a reflected wave at a frequency $f$ at a certain observer position, then the complex pressure amplitude is given by

$$\begin{aligned} p_d &= |p_d|\, e^{-i\omega(t-t_d)} \\ p_r &= |p_r||R_p|\, e^{i\xi} e^{-i\omega(t-t_r)} \end{aligned} \tag{36}$$

where the $|p_d|$ and $|p_r|$ is obtained by the pressure amplitude evaluation outlined in section 4.3.

$$|p_d + p_r|^2 = |p_d|^2 + |R_p|^2 |p_r|^2 + 2|R_p||p_d||p_r| I \tag{37}$$

where $I$ is a measure for the amount of destructive or constructive interference. For discrete frequencies

$$I = \cos(\omega\Delta t + \xi) \tag{38}$$

**Table 1: Table of flow resistivity data of various natural occurring ground surfaces**

| Type of ground surface | σ [Pa s/m$^2$] |
|---|---|
| Concrete | 65 . $10^6$ |
| Asphalt, old, sealed with dust | 27 . $10^6$ |
| Asphalt, new, varies with particle size | 10 . $10^6$ |
| Dirt, exposed, rain-packed | 6 . $10^6$ |
| Sand, various types | 317 . $10^3$ |
| Grass lawn or grass field | 200 . $10^3$ |
| Grass field, 16.5% moisture content | 75 . $10^3$ |
| Forest floor (pine/hemlock) | 50 . $10^3$ |
| Grass field, 11.9% moisture content | 41 . $10^3$ |

, and when considering 1/3 octave band centre frequencies $f_c$

$$I = \frac{\sin\left(0.727 f_c \Delta t\right)}{0.727 f_c \Delta t} \cos\left(6.325 f_c \Delta t + \xi\right) \tag{39}$$

In eq. (38) and eq. (39) $\Delta t = t_r - t_d$. For rays that reach the observer by multiple reflections one can expect that the coherence loss is substantial. Therefore it is suggested to add them incoherently to the total acoustic pressure level.

# 5. MODEL EVALUATION

## 5.1. Effects of the atmosphere on sound propagation

The effect of a realistic atmosphere on noise propagation is assessed. A comparison is made between an atmosphere with constant temperature and velocity, a decreasing temperature (–0.0065°K/m, ISA) and finally, an atmosphere with wind with a logarithmic velocity profile.

Figure 10 plots the transmission loss at a frequency of $f$ = 1kHz for a source located at the origin at an altitude of 300m. For an atmosphere with constant temperature and wind velocity (left contour) a logarithmic decay (spherical spreading) is found near to the source which becomes progressively more linear (atmospheric attenuation) for distances far away from the source. Furthermore a pattern of constructive and destructive interference is displayed due to presence of an impedance surface.

For the case of decreasing temperature with altitude a similar footprint is found. The interference pattern is affected for ray paths that are orientated nearly parallel to the surface. For this condition refraction is the strongest and the curvature of the ray paths causes a change in wave front travel time. The effect on the spreading rate itself is limited.

The introduction of wind has a profound effect on noise propagation. The footprint and interference pattern is no longer axisymmetric. In the wind upstream direction

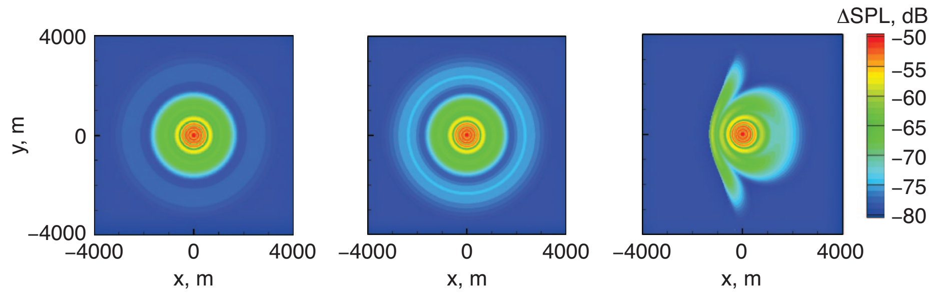


**Figure 10:** The effect of the atmosphere on transmission loss, left: constant temperature no wind, centre: descreasing temperature with altitude (–0.0065°K/m), right: logarithmic wind profile ($v_{10}$ = 7m/s), $f$ = 1kHz, $Z_{scr}$ = 300m.

(x~1200m) a shadow zone exists where rays cannot reach, which causes an area of strongly attenuated noise levels. The refraction due to wind affects the spreading rate significantly. Due to divergence of the ray paths in the downwind direction the spreading rate increases. For example at x = 1500m and at x = 3000m an additional attenuation of respectively –1dB and –3dB is found with respect to spherical spreading. Inversely, in the upwind direction, approaching the shadow zone, a focusing of rays occurs that results in a decrease of attenuation (+3dB).

## 5.2. Cross validation

In this section two benchmarks will be discussed for which a cross-validation is performed against independently developed ray tracing procedures[13, 14].

The first case considered is a source at 300m altitude, in an atmosphere with linearly decreasing temperature (–0.01°K/m) and a logarithmic velocity profile ($v_{10}$ = 7m/s) as shown in Figure 11. Ground reflections and atmospheric attenuation is not considered in order to retain focus on the ray tracing algorithms. The results are compared with the ray tracing model by Olsman et al. [13] as shown in Figure 12.

From the contour plot and line plot it is seen that the results are near identical. Section 4.1 states that the out-of-plane ray displacement is negligible. To assess the validity of this assumption, the out-of-plane ray displacement is calculated based on eq. (24), where instead of $c_s$ the plane normal component of velocity is inserted. From the out-of-plane displacement a corrected X-Y observer position is calculated. This was used for the contour plot in Figure 12. The results show a minor effect and therefore confirming that it is acceptable to neglect the out-of-plane displacement.

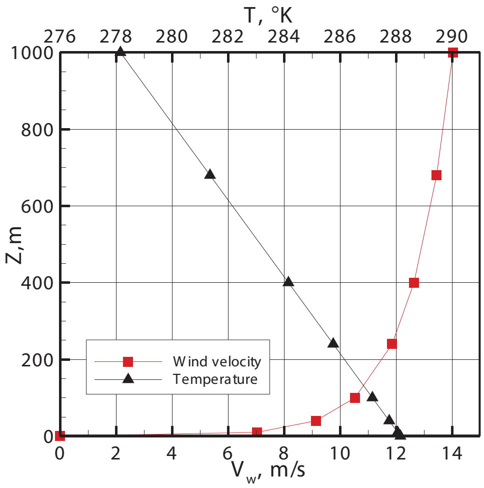


| $Z$, m | $V_w$, m/s | $T$, ºK |
|---|---|---|
| 0 | 0.0 | 288.15 |
| 10 | 7.0 | 288.05 |
| 40 | 9.1 | 287.75 |
| 100 | 10.5 | 287.15 |
| 240 | 11.9 | 285.75 |
| 400 | 12.6 | 284.15 |
| 680 | 13.4 | 281.35 |
| 1000 | 14.0 | 278.15 |

**Figure 11:** Temperature and wind input for cross-validation benchmark 1.

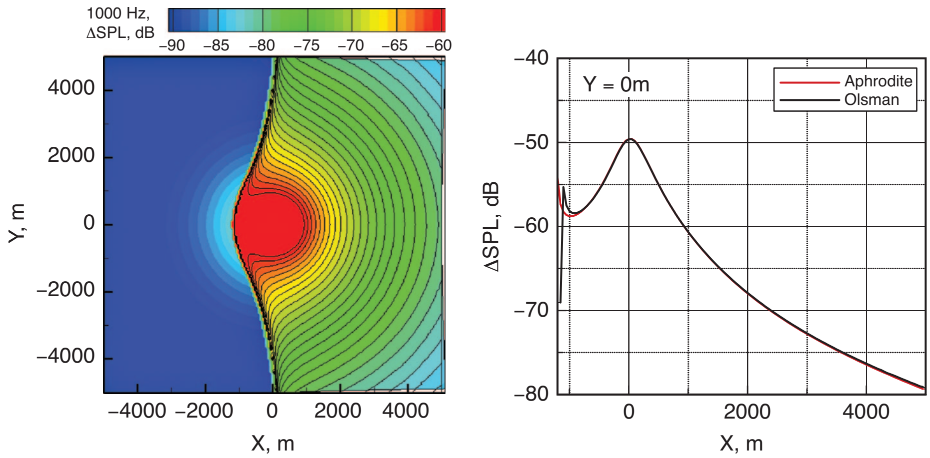


**Figure 12:** Transmission loss at 1kHz, left: Contour plot in which the colors are APHRODITE output and the lines are obtained from the Olsman model., right: line plot obtained at Y = 0m.

A second benchmark is considered with an emphasis on long-range-propagation, required to assess e.g. enroute noise (NINHA project). The source is located at an altitude of 9500m. The temperature and velocity profile in the atmosphere are given in Figure 13.

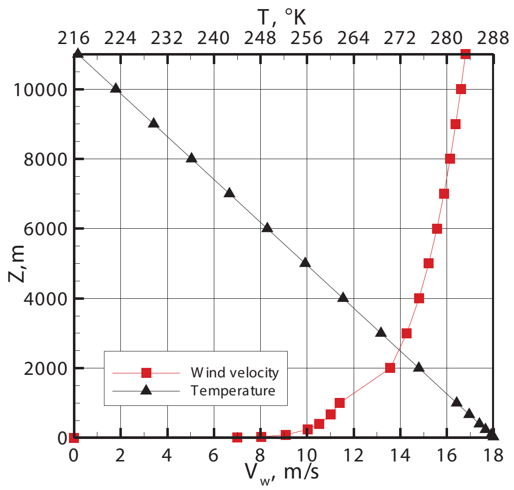


| $Z$, m | $V_w$, m/s | $T$, °K |
|---|---|---|
| 0 | 0.0 | 288.15 |
| 10 | 7.0 | 288.10 |
| 30 | 8.0 | 287.97 |
| 90 | 9.1 | 287.58 |
| 240 | 10.0 | 286.60 |
| 400 | 10.5 | 285.56 |
| 670 | 11.0 | 283.81 |
| 1000 | 11.4 | 281.66 |
| 2000 | 13.6 | 275.16 |
| 3000 | 14.3 | 268.66 |
| 4000 | 14.8 | 262.16 |
| 5000 | 15.2 | 255.66 |
| 6000 | 15.6 | 249.16 |
| 7000 | 15.9 | 242.66 |
| 8000 | 16.1 | 236.16 |
| 9000 | 16.4 | 229.66 |
| 10000 | 16.6 | 223.16 |
| 11000 | 16.8 | 216.66 |

**Figure 13:** Temperature and wind input for cross-validation benchmark 2.

For the second benchmark, atmospheric attenuation and ground reflection is considered as well. A constant relative humidity is assumed of 70%. Furthermore, a soft surface with a flow resistivity of $\sigma = 50000$ Pa s/m$^2$ is defined at Z = 0m. The outcome of the simulations is shown in Figure 14, where it is compared with the Raytrac ray tracing model by Brouwer [14].

The contour plot shows that the results are generally in good agreement. Investigation of the line plot at y = 0m reveals that for –12 km < x < 12 km the discrepancies are small and in the order of 1.5dB. Outside this range more significant discrepancies are displayed. The shadow zone occurs approximately 5 km earlier for the Raytrac and in the downwind direction rays diverge faster, resulting in a higher transmission loss.

Although of little practical relevance (transmission losses are larger than 120dB), a hypothesis is formulated on the cause of these discrepancies. Raytrac applies a spline fit on the velocity profile given as input, whereas APHRODITE assumes a linear dependency within a layer. In particular near the surface where gradients are large this can result in marginally different velocity profiles, potentially affecting near horizontal rays significantly since the radius of curvature of the rays will change. The expected outcome would be a different shadow zone location and a different spreading rate, as is shown in Figure 13. This hypothesis is tested by performing a Raytrac calculation with 100 segments, matching the linear varying profile of APHRODITE, of which the results are shown by the dash-dot line in Figure 13 - right. Now, for –12 km < x < 12 km the results show little discrepancies, the shadow zone occurs at the same location and the spreading rate in the downwind direction matches closely.

The original discrepancies reveal a sensitivity of ray limiting behavior to minute changes in the input that defines the large gradient in wind velocity that occurs near the

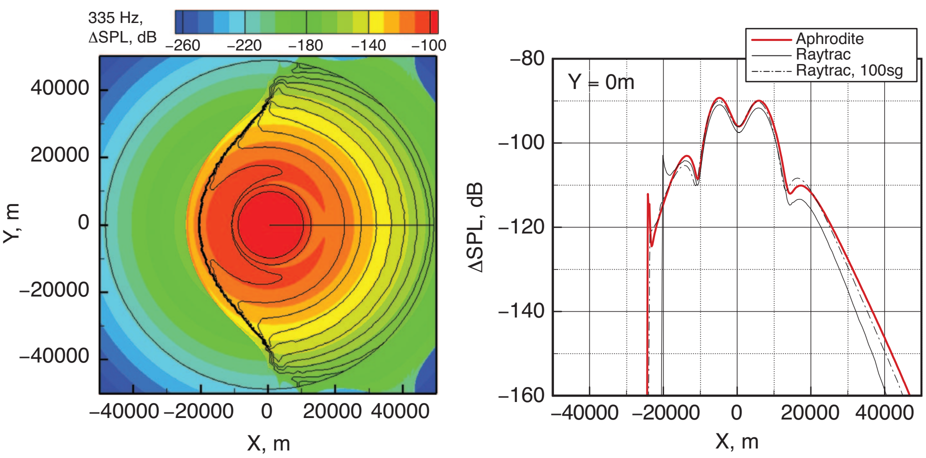


**Figure 14:** Transmission loss at 335Hz, left: Contour plot in which the colors are APHRODITE output and the lines are obtained from the Raytrack model., right: line plot obtained at Y = 0m.

surface, irrespective of ray tracing model that is used. This observation leads to a more fundamental question if ray tracing is adequate in the surface region at all, since the base assumption that changes in the medium occur at a scale far greater than an acoustic is violated.

## 5.3. Performance evaluation

One of the objectives is to provide a computationally lean routine for atmospheric noise propagation. Therefore, in this section the performance is assessed in terms of required computational time and calculation time per ray.

The second benchmark as presented in section 5.2 is considered. The spatial resolution is progressively increased for a rectangular grid of observers covering an area of 50 km × 50 km on the ground. The total time and time per ray needed to perform the calculation is shown in Figure 15.

The total calculation time increases approximately linear with the number of observers. As a consequence the time required per ray is approximately constant. Figure 15 contains results for four types of CPU:

- a low-end dual core Celeron 847 processor,
- a mid-range dual core intel i5 M560 processor,
- a high-end quad core i7 3630QM processor and
- a high-end octa-core Xeon E5-2650 V2 processor

RAM memory is not considered to be a limitation. The algorithm performs well even on a Celeron processor (50ms per ray). The high-end processors perform approximately 10 times faster (5μs per ray). The benefit of the octacore processor with respect to the i7 quad-core is only apparent for higher number of observers ($>2\cdot10^5$) where calculation time per ray is reduced to about 3μs per ray.

When calculation time is concerned, the number of segments used to discretise the atmosphere is another parameter that is expected to be of relevance. Therefore,

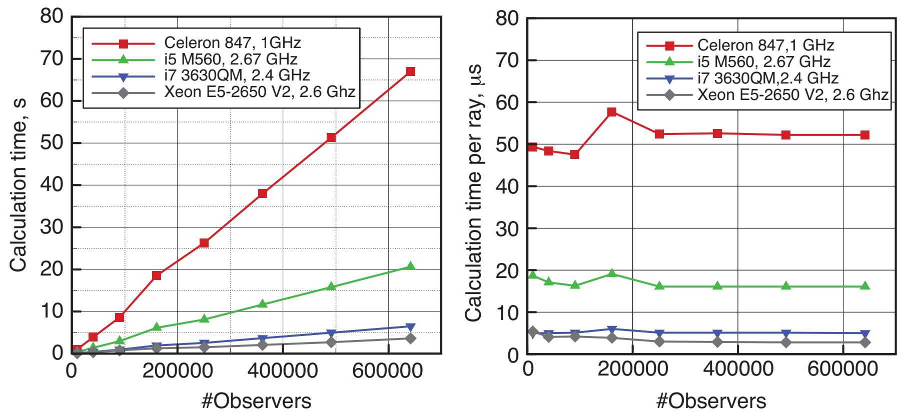


**Figure 15:** The effect of the number of observers (virtual microphones) on calculation time, left: total calculation time, right calculation time per ray.

in order to assess the impact on calculation time the layers are progressively merged, starting from 18 segments to a minimum of 2 segments. The results of this exercise are given in Figure 16.

Again an approximately linear relation between calculation time and the number of segments is found. However, this time it is due to an increase in calculation time per ray. An exception to this rule is found for the reduction from 4 to 2 segments, which does not impact calculation time significantly.

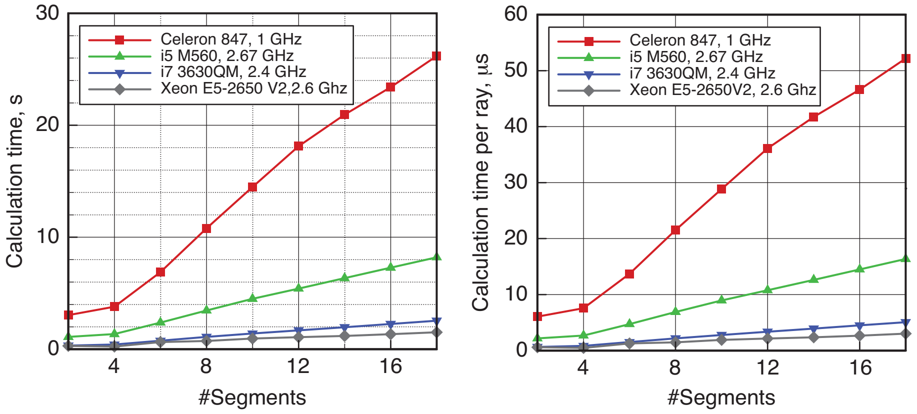


**Figure 16:** The effect of the number of the number of segments on calculation time, left: total calculation time, right calculation time per ray ($500^2$ observers).

## 6. CONCLUSIONS

A robust and computationally lean method to incorporate the effects of the atmosphere on noise propagation for aircraft noise modelling was developed.

From the Eikonal equation follows that a ray obeys to an adapted form of Snell's law, when the wave front orientation is approximated to be orientated perpendicular to the ray path. Furthermore, a key assumption is that speed of sound and velocity may be described as linearly varying within an atmospheric layer. This allows the ray path and ray properties to be described analytically, from which the method derives its low calculation times.

An efficient ray matching algorithm was devised in order to find the ray path to a desired observer location. The adapted form of Snell's law allows finding the ray launch angle at which a shadow zone first occurs a-priory. In case the observer is not located in the shadow zone a solution is readily found by application of standard rout-solver algorithms.

A cross-validation was performed with two independently developed ray tracing routines, which showed a good agreement of the benchmark results.

## ACKNOWLEDGMENTS

This research is supported by the European Seventh Framework Programme (FP7/2007-2013) under the NINHA project (Noise Impact of aircraft with Novel engine configurations in mid- to High Altitude operations).

## REFERENCES

[1] SAE, "Prediction Method of Lateral Attenuation of Airplane Noise During Takeoff and Landing", AIR 1751, 1981.

[2] Standard Atmosphere, ISO 2533:1975.

[3] A.S Monin. and A.M. Obukhov, "Basic laws of turbulent mixing in the atmosphere near the ground", Tr. Akad. Nauk., SSSR geophiz inst., no. 24(151), p. 1963–1987, 1954.

[4] R.B. Bull, "An introduction to boundary layer meteorology", atmospheric sciences library, 1988.

[5] A.P. Dowling and J.E. Ffowcs William, ,"Sound and sources of sound", 1983.

[6] A.D. Pierce, "Acoustics, an introduction to its physical principles an applications", 1981.

[7] R.P. Brent, "Algorithms for Minimization without Derivatives", Englewood Cliffs, Chapter 4, NJ: Prentice-Hall, 1973.

[8] H.E. Bass, L.C. Sutherland, A.J. Zuckerwar, D.T. Blackstone and D.M. Hester, Atmospheric absorption of sound: Further developments, JASA, Vol. 97, No.1, pp. 680–683, 1995.

[9] SA E Standard Values of Atmospheric Absorption as a Function of Temperature and Humidity, SAE-ARP-866A, March 1975.

[10] ANSI S1.26-1995 "Method for the calculation of the absorption of sound by the atmosphere", 1995.

[11] M.E. Delaney and E.N. Bazley, "Acoustic properties of fibrous absorbent materials", Appl. Acoust., Vol. 3, pp. 105–0116, 1970.

[12] K. Attenborough, I. Bashir and S. Taherzadeh, "Review of ground impedance models for propagation modelling", 3:1836–1845, 39th Internoise conference, 2010.

[13] W.F.J. Olsman and M.Lummer, "Influence of wind on the noise footprint of a helicopter landing", 38th European Rotorcraft Forum, Amsterdam, ERF-2012–046, 2012.

[14] H.H. Brouwer, "A ray acoustics model for the propagation of aircraft noise through the atmosphere", International Journal of Aeroacoustics, this issue, 2014 (To-be-published).

## APPENDIX

This appendix provides a list of standard integrals that are a function of

$$R = \sqrt{ax^2 + bx + c} \tag{40}$$

$$\int \frac{dx}{R} = \begin{cases} \frac{1}{\sqrt{a}} \ln\left|2\sqrt{a}R + 2ax + b\right| & \text{if} \quad a > 0 \\ -\frac{1}{\sqrt{-a}} \arcsin \frac{2ax+b}{\sqrt{b^2 - 4ac}} & \text{if} \quad a < 0 \quad \text{and} \quad b^2 - 4ac > 0 \\ \frac{1}{\sqrt{a}} \operatorname{arcsin h}\left(\frac{2ax+b}{\sqrt{4ac - b^2}}\right) & \end{cases} \tag{41}$$

$$\int \frac{x}{R} dx = \frac{R}{a} - \frac{b}{2a} \int \frac{dx}{R} \tag{42}$$

$$\int \frac{x^2}{R} dx = \frac{2x - 3b}{4a^2} R + \frac{3b^2 - 4ac}{8a^2} \int \frac{dx}{R} \tag{43}$$

$$\int \frac{dx}{xR} = \begin{cases} -\frac{1}{\sqrt{c}} \ln\left|\frac{2\sqrt{cR + bx + 2c}}{x}\right| & \text{if} \quad c > 0 \\ \frac{1}{\sqrt{-c}} \arcsin \frac{bx + 2c}{|x|\sqrt{b^2 - 4ac}} & \text{if} \quad c > 0 \\ -\frac{1}{\sqrt{c}} \operatorname{arcsin h}\left(\frac{bx + 2c}{|x|\sqrt{4ac - b^2}}\right) & \end{cases} \tag{44}$$